

Original Article

Cite this article: Huang J, Chen Y, Chu X, and Sun T (2019) The geochemistry of the late Cambrian carbonate in North China: the Steptoean Positive Carbon Isotope Excursion (SPICE) record suppressed in a coastal condition? *Geological Magazine* **156**: 1805–1819.
<https://doi.org/10.1017/S0016756819000025>

Received: 24 May 2018

Revised: 29 October 2018

Accepted: 9 January 2019

First published online: 8 March 2019


Keywords:

carbon isotope; sulphur isotope; terrigenous input; trace element

Author for correspondence: Jing Huang,

Email: hjmail@ustc.edu.cn

The geochemistry of the late Cambrian carbonate in North China: the Steptoean Positive Carbon Isotope Excursion (SPICE) record suppressed in a coastal condition?

Jing Huang^{1,2} , Yali Chen³, Xuelei Chu^{4,5} and Tao Sun⁶

¹CAS Key Laboratory of Crust-Mantle Materials and Environments, School of Earth and Space Sciences, University of Science and Technology of China, Hefei 230026, China; ²CAS Center for Excellence in Comparative Planetology, China; ³Agro-Environmental Protection Institute/Key Laboratory for Environmental Factors Control of Agro-product Quality Safety, Ministry of Agriculture and Rural Affairs, Tianjin 300191, China; ⁴Institute of Geology and Geophysics, Key Laboratory for Mineral Resources, Chinese Academy of Sciences, Beijing 100029, China; ⁵University of Chinese Academy of Sciences, Beijing 100049, China and ⁶Department of Earth, Environmental and Planetary Sciences, Rice University, Houston, TX 77005, USA

Abstract

The Steptoean Positive Carbon Isotope Excursion (SPICE) is globally distributed in late Cambrian sedimentary records but controversially heterogeneous in its magnitudes. Here we use multiple geochemical proxies to investigate the late Cambrian carbonates from the Tangwangzhai section in North China, which were deposited in a shallow coastal environment with three depositional sequences (S1–S3). Each sequence comprises a transgressive systems tract (TST) and a highstand systems tract (HST). The REE + Y and trace element records are consistent with the depositional condition and indicate that terrigenous influence was more significant in the TST than HST. $\delta^{13}\text{C}_{\text{carb}}$ and $\delta^{34}\text{S}_{\text{CAS}}$ are low in the TST relative to HST, consistent with the scenario that terrigenous inputs were profoundly aggressive to seawater by introducing ^{13}C -depleted and ^{34}S -depleted materials. Within the TST of S2, the SPICE excursion shows a scaled-down $\delta^{13}\text{C}_{\text{carb}}$ positive shift ($\sim 1.7\text{‰}$) relative to its general records ($\sim 4\text{--}6\text{‰}$); the corresponding $\delta^{34}\text{S}_{\text{CAS}}$ show no positive excursion. This ‘atypical’ SPICE record is attributed to enhanced ^{13}C -depleted and ^{34}S -depleted terrigenous influence during the TST, which would reduce the amplitude of $\delta^{13}\text{C}_{\text{carb}}$ excursion, and even obscure $\delta^{34}\text{S}_{\text{CAS}}$ excursion. Meanwhile the subaerial unconformity at the base of TST would also cause a partially missing and a ‘snapshot’ preservation. Our study confirms significant local influence to the SPICE records, and further supports the heterogeneity and low sulphate concentrations of the late Cambrian seawater, because of which the SPICE records may be vulnerable to specific depositional conditions (e.g. sea-level, terrigenous input).

1. Introduction

A series of geochemical perturbations were recorded in the late Cambrian stratum, of which the Steptoean Positive Carbon Isotope Excursion (SPICE) is one of the most intriguing and yet puzzling records because of its dramatic shifts in both carbon and sulphur isotope, worldwide distributions, implications of ocean/atmosphere redox changes, and close connections with the biological extinction/turnover (Saltzman *et al.* 2000, 2011; Gill *et al.* 2007, 2011; Hurtgen *et al.* 2009; Maloof *et al.* 2010). The SPICE started at the base of the Paibian Stage, Furongian Series (~ 499 Ma), and lasted for 2–4 Ma (Peng *et al.* 2012), which shows a distinct record of 4–6 ‰ positive shift in the carbon isotope of carbonate ($\delta^{13}\text{C}_{\text{carb}}$) in the strata from Antarctica, Argentina, Australia, England, Poland, France, Spain, Wales, Kazakhstan, Newfoundland, South China, Siberia, Sweden and the USA (Saltzman *et al.* 1998, 2004; Zhu *et al.* 2004; Cowan *et al.* 2005; Álvaro *et al.* 2007; Glumac & Mutti, 2007; Ahlberg *et al.* 2009; Gill *et al.* 2011; Glumac, 2011; Woods *et al.* 2011; Peng *et al.* 2012; Sial *et al.* 2013; Wotte & Strauss, 2015). A covariation between the SPICE and organic carbon isotopic composition ($\delta^{13}\text{C}_{\text{org}}$), or the sulphur isotopic composition (carbonate-associated sulphate ($\delta^{34}\text{S}_{\text{CAS}}$) and sedimentary pyrite ($\delta^{34}\text{S}_{\text{py}}$)) was also reported (Gill *et al.* 2011; Saltzman *et al.* 2011). The parallel positive carbon and sulphur isotope excursions contradict their general inverse relationship, which is considered as the first-order long-term relationship of marine carbon and sulphur isotope throughout the Phanerozoic (Veizer *et al.* 1980; Garrels & Lerman, 1981). This SPICE anomaly is thought to reflect a superimposed shorter-term variability that was caused by enhanced burial of organic carbon and pyrite (Gill *et al.* 2007), which has been proposed to be driven by sea-level changes, seawater warming or spread of euxinia (Saltzman *et al.* 2000, 2004, 2011; Cowan *et al.* 2005; Elrick *et al.* 2011; Gill *et al.* 2011; Dahl *et al.* 2014). The SPICE

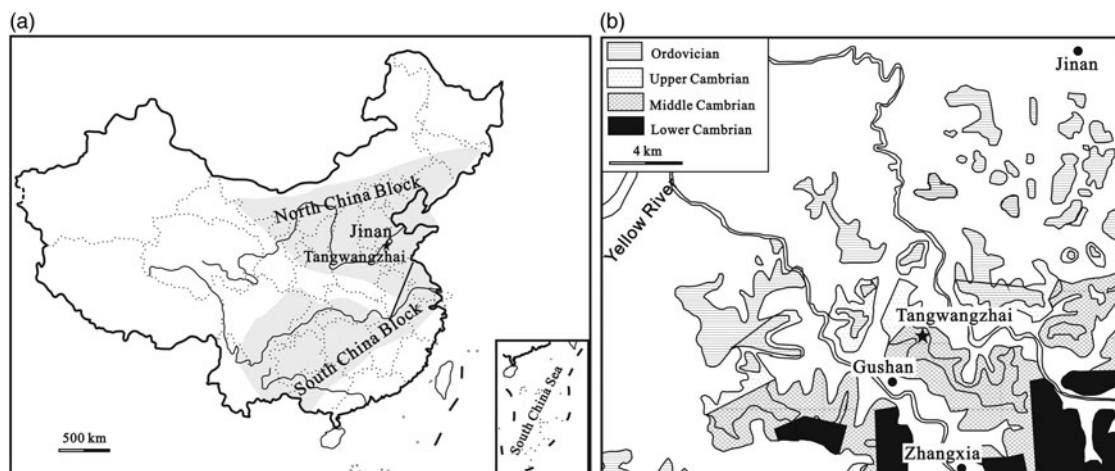


Fig. 1. (a) The study regions in China (modified from Zhu *et al.* 2004); (b) geological map of the Tangwangzhai section.

was also thought to have ties to the changes in atmosphere/ocean redox conditions: widespread anoxic and even euxinic conditions in the ocean contributed in the enhanced burial of organic carbon and pyrite, and might be associated with the trilobite extinction/turnover events at the beginning of SPICE (Peng *et al.* 2004; Gill *et al.* 2011; Dahl *et al.* 2014); elevated rates of organic carbon and pyrite burial led to a significant rise in atmospheric oxygen concentration (Berner, 2006; Saltzman *et al.* 2011), and triggered the onset of 'Plankton Revolution' after the SPICE (Saltzman *et al.* 2011).

Recent studies showed differences in onset, peak values and pattern of the $\delta^{13}\text{C}_{\text{carb}}$ and $\delta^{34}\text{S}_{\text{CAS}}$ excursions for SPICE in different regions, and even missing of the excursions in some regions, reflecting the heterogeneity of late Cambrian seawater in carbon and sulphur isotopic compositions (Saltzman *et al.* 1998; Hurtgen *et al.* 2009; Gill *et al.* 2011; Wotte & Strauss, 2015; Schiffbauer *et al.* 2017; Li *et al.* 2018). Various mechanisms were proposed to explain these variations in $\delta^{13}\text{C}_{\text{carb}}$ and $\delta^{34}\text{S}_{\text{CAS}}$ excursions. Sedimentary studies showed that the existence of a sedimentary hiatus would cause the SPICE excursion to be missing (or partially missing) in some regions, such as northwestern Wyoming, northern Vermont and North China (Saltzman *et al.* 1998; Glumac & Spivak-Birndorf, 2002; Chen *et al.* 2011). The invasion of deep ^{13}C -enriched water during the Sauk III transgression would produce the gradients of $\delta^{13}\text{C}_{\text{carb}}$ amplitude and SPICE stratigraphic thicknesses across the different depths (Schiffbauer *et al.* 2017). Low-level sulphate in the late Cambrian ocean would make the sulphate reservoir more sensitive to the change in local depositional conditions (Hough *et al.* 2006; Gill *et al.* 2007, 2011; Hurtgen *et al.* 2009; Wotte & Strauss, 2015), leading to variable sulphur isotopic records as well.

The late Cambrian succession is well developed in North China, where the sedimentary record and palaeontology have been well studied (Zhu *et al.* 2004; Peng, 2007, 2009a, b; Chough *et al.* 2010; Lee *et al.* 2010; Chen *et al.* 2011, 2012; Zhou *et al.* 2011; Ng *et al.* 2015). The biostratigraphic correlation with that in other parts of the world is also well constrained (Peng, 2009a, b; Chough *et al.* 2010; Ng *et al.* 2015). A carbon isotopic positive excursion in the late Cambrian carbonate was identified as the SPICE record in North China in recent studies (Zhu *et al.* 2004; Bagnoli *et al.* 2014; Ng *et al.* 2014a, b). Compared with other regions, the SPICE records in North China are always in a thinner succession (~5–20 m), and some of the carbon isotope shifts are relatively small (<2.5 ‰ compared with 4–6 ‰) (Ng *et al.* 2014a, b). This 'atypical SPICE' record in North China likely provides an opportunity to explore the wide

variation in sulphur and carbon isotopic behaviour during the SPICE, for which much of the geochemical information is still insufficient to constrain the depositional conditions, sizes of dissolved inorganic carbon (DIC)/oceanic sulphate and decoupling between C/S cycles, etc.

In this study, we investigate late Cambrian carbonate from the Tangwangzhai section in Shandong Province using multiple geochemical proxies (e.g. $\delta^{13}\text{C}_{\text{org}}$, $\delta^{34}\text{S}_{\text{CAS}}$ and trace elements). The trace element results illustrate the depositional condition changes during the late Cambrian in North China. The carbon and sulphur isotopic records provide insights for stratigraphic correlation of the global SPICE and explore the competing influence between global ocean chemistry and local influx on the carbon isotopic signatures.

2. Geological background

The middle and late Cambrian succession in Shandong Province is composed of the Liguan, Zhushadong, Mantou, Zhangxia, Gushan and Chaomidian formations (from bottom to top), which mainly consist of marine-origin carbonates and thinly interbedded shales (Chough *et al.* 2010; Chen *et al.* 2011; Lee *et al.* 2012, 2014). The Tangwangzhai section is the type section for the late Cambrian sequence in North China, consisting of the Zhangxia, Gushan and Chaomidian formations, and it is located near Tangwangzhai Village, south of Jinan, Shandong Province (Fig. 1). The upper Zhangxia Formation mainly consists of bioclastic limestone and oolitic limestone with intercalations of calcareous shale, and it contains the trilobite *Yabeia*–*Damesella* Zone; the Gushan Formation (~52 m thickness) mainly consists of flat-pebble grainstone, thinly bedded micrites and yellowish-green calcareous shale, and it contains the trilobite *Blackwelderia* and *Neodrepanura* zones; the Chaomidian Formation (~160 m thickness) consists of oolitic limestone, thinly bedded micrites, flat-pebble grainstone and yellowish-green calcareous shale, and it contains the trilobite *Chuangia*, *Changshania*–*Irvingella*, *Kaolishania* and *Ptychaspis*–*Tsinania* zones (Zhu *et al.* 2004; Bagnoli *et al.* 2014) (Fig. 2).

Chen *et al.* (2011) identified three third-order depositional sequences (S1–S3) for the succession in the Tangwangzhai section (Fig. 2). Each sequence comprises a transgressive systems tract (TST) and a highstand systems tract (HST). The sediments in the TST contain more detrital components (e.g. shale and mudstone interlayers) (Fig. 2). It has been suggested that S1 and S2 are bounded by a subaerial unconformity (BS2) at the boundary

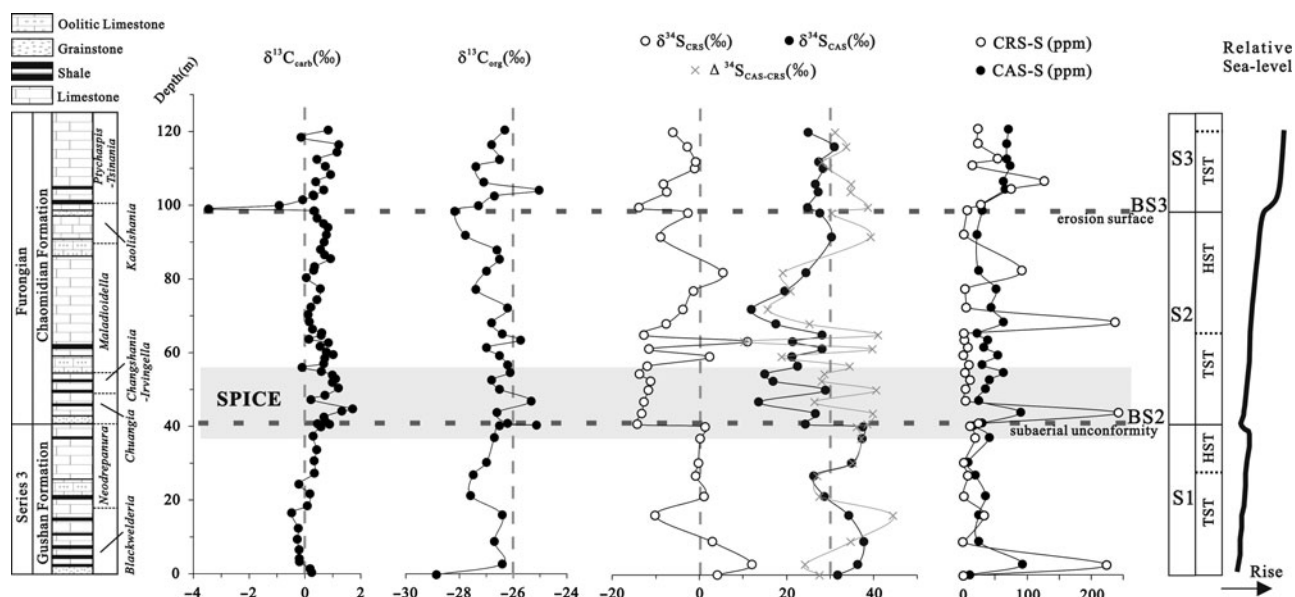


Fig. 2. The stratigraphic column and carbon and sulphur isotopic composition variations from late Cambrian carbonate in the Tangwangzhai section. The relative sea-level curve is after Chen *et al.* (2011). Both carbon and sulphur isotope show fluctuant, in which the $\delta^{13}\text{C}_{\text{carb}}$ shows a mild positive excursion between 40 and 60 m, while the $\delta^{34}\text{S}_{\text{CAS}}$ and $\delta^{34}\text{S}_{\text{py}}$ do not show synchronous increase.

between the Gushan Formation and the Chaomidian Formation, and S2 and S3 are bounded by a surface of submarine erosion (BS3) in the middle of the Chaomidian Formation (Chen *et al.* 2011, 2012) (Fig. 2). The boundary is characterized by predominant grainstone facies with fragmentary bioclasts, ooids, peloids, intraclasts and abundant glauconite grains (Fig. 2) (Chen *et al.* 2011, 2012; Lee *et al.* 2012, 2014). These fundamental researches are conducive to the stratigraphic correlation and integrated consideration of the environmental changes during the late Cambrian.

3. Methods

We collected large carbonate hand-specimens from outcrops to ensure sufficient quantities for geochemical analysis. The samples were cut and buffed to remove weathered surfaces and secondary veins and were then ground (<200 mesh) in an agate mortar for elemental and isotopic analyses.

For the $\delta^{13}\text{C}_{\text{carb}}$ analyses, the carbonate samples were roasted and were then reacted with concentrated H_3PO_4 at 25 °C for 24 h, and the liberated CO_2 was collected cryogenically off-line under vacuum and sealed in a Pyrex tube. We measured carbon and oxygen isotope ratios on a Thermo MAT 253 gas source isotope ratio mass spectrometer; the isotopic compositions are reported in units of per mil (‰) as deviations relative to that of Vienna Pee Dee Belemnite (VPDB) using the conventional delta ($\delta^{13}\text{C}$ and $\delta^{18}\text{O}$) notations. The standard GBW4405 was used to control the analytical uncertainties, which were better than ± 0.10 ‰ (1 σ) for both $\delta^{13}\text{C}$ and $\delta^{18}\text{O}$. The isotope analysis was conducted at the State Key Laboratory of Lithospheric Evolution, Institute of Geology and Geophysics, Chinese Academy of Sciences (Beijing, China).

For the $\delta^{13}\text{C}_{\text{org}}$ analyses, powdered samples were first decarbonated by reacting with HCl (1 M), and the residual was rinsed at least six times with deionized distilled (DD) water and dried. The decarbonated samples were enclosed in tin capsules, and the organic carbon isotopes were analysed using an elemental analyser (EA) coupled with a conflo interface that automatically transfers carbon

dioxide gas into a Thermo MAT 253 gas source isotope ratio mass spectrometer (Biogeochemistry Laboratory of University of Science and Technology of China (USTC), Hefei, China). The analytical uncertainties set from replicate analyses of standards (IAEA-600 and USGS-40) is better than ± 0.15 ‰ (1 σ ; SD).

The carbonate-associated sulphate (CAS) was extracted following the method described in the previous work (Gill *et al.* 2011). Fifty grams of sample was first rinsed with 10 % NaCl solution (overnight under agitation) to remove the non-CAS sulphate and then treated with 5.25% NaClO solution to remove organic sulphur and sulphide minerals. Samples were rinsed with DD water six times, then dissolved with 6 M HCl quickly (within 20 min). The solution was filtered, and CAS was precipitated as BaSO_4 with the addition of 20 mL BaCl_2 solution (100 g L^{-1}). The precipitates were collected by filtration and then washed with DD water. The BaSO_4 was dried and weighed (precision, 0.0001 g). CAS concentrations were determined gravimetrically with an analytical uncertainty of 10 %. Approximately 15 mg BaSO_4 was mixed with V_2O_5 (150 mg) and SiO_2 (150 mg) and combusted at 1100 °C. The produced SO_2 was passed through a copper column at 600 °C, and then cryogenically collected off-line to a Pyrex tube. Measurements of the SO_2 sulphur isotope ratios were performed on a Delta S isotope ratio mass spectrometer in a dual inlet mode. Sulphur isotope compositions are reported in units of per mil (‰) as deviations relative to that of Vienna Canon Diablo Troilite (VCDT) using the conventional delta ($\delta^{34}\text{S}$) notation. A laboratory internal standard SA1 (barite, with $\delta^{34}\text{S}$ of 15.2 ± 0.2 ‰) was used as quality control to monitor the analysing system. The isotope analysis was performed at the State Key Laboratory of Lithospheric Evolution, Institute of Geology and Geophysics, Chinese Academy of Sciences. The analytical uncertainties were better than ± 0.2 ‰ (1 σ).

To evaluate the completion of the removal of non-CAS by NaCl, 5–20 g of samples were leached by 10% NaCl overnight under continuous agitation, and the leached sulphate was tested by adding saturated barium chloride solution (BaCl_2) to precipitate barite (Wotte *et al.* 2012a). For most samples, no leachable non-CAS was detected after the first or second NaCl leaching, indicating that

one-time NaCl leaching is adequate to prohibit leachable non-CAS contributions for our samples.

Then the leached samples were acidized by 25 % HCl, and the insoluble residue was used to extract the chromium-reducible sulphur (CRS) following the previous procedure (Arnold *et al.* 2014). The Ag₂S was dried and weighed (precision 0.0001 g). CRS concentrations were determined gravimetrically with an analytical uncertainty of 10 %. The $\delta^{34}\text{S}_{\text{CRS}}$ was measured by online combustion of Ag₂S precipitates with an excess of V₂O₅ on a Thermo Delta V Plus isotope ratios mass spectrometer coupled with a Costech elemental analyser. Sulphur isotopes are reported in standard δ -notation relative to Vienna Canon Diablo Troilite (VCDT). Analytical precision for $\delta^{34}\text{S}_{\text{CRS}}$ of the sample set from replicate analyses of IAEA standards (IAEA S1, S2 and S3) is better than ± 0.2 ‰ (1 σ ; SD).

The major elements of the bulk samples were analysed using X-ray fluorescence spectrometry (XRF) with a Shimadzu XRF-1500 system (State Key Laboratory of Lithospheric Evolution, Institute of Geology and Geophysics, Chinese Academy of Sciences); we used fusion glasses made from a mixture of sample powder and flux (Li₂B₄O₇) at a ratio of 1:5. The analytical precision monitored by an internal standard was better than 10% (1 σ).

For trace elemental analyses, 40 mg of sample powder was reacted with 1 mL of 1 M acetic acid in a Teflon pot for 4 h and was then centrifuged. Insoluble residues were removed by filtration, dried and reweighed. The supernatant was dried, re-dissolved in 0.5 mL of 0.1 M HNO₃ and dried again. This process was repeated until all of the acetic acid was removed. The sample was then dissolved in 1 % HNO₃. The final solutions were analysed for trace element (including rare earth element (REE)) concentrations on an inductively coupled plasma mass spectrometer (ICP-MS) monitored by an internal standard (In) using a Finnigan MAT Element system (State Key Laboratory of Lithospheric Evolution, Institute of Geology and Geophysics, Chinese Academy of Sciences). The analytical precision monitored by the internal standard was better than 10 % (1 σ) for trace elements.

4. Results

The carbon and sulphur isotopic compositions are listed in Table 1 and plotted in Figure 2. The $\delta^{13}\text{C}_{\text{carb}}$ in S1 mostly ranges between -0.50 ‰ and 0.86 ‰ and slightly increases from the bottom up. The $\delta^{13}\text{C}_{\text{carb}}$ shows a positive excursion around BS2 (~ 40 – 50 m), and the highest value approaches 1.68 ‰. Afterwards, the $\delta^{13}\text{C}_{\text{carb}}$ decreases (down to 0 ‰) to the middle of S2 (~ 50 – 70 m) and then increases and fluctuates around 0.5 ‰ in the upper part of S2 (~ 70 – 98 m). An abrupt decline of the $\delta^{13}\text{C}_{\text{carb}}$ (down to -3.48 ‰) appears at BS3 (at ~ 100 m). Then the $\delta^{13}\text{C}_{\text{carb}}$ increases and fluctuates around 1 ‰ in S3 (above 100 m). The $\delta^{13}\text{C}_{\text{org}}$ ranges between -28.9 ‰ and -25.0 ‰. The $\delta^{13}\text{C}_{\text{org}}$ increases abruptly (up to -25 ‰) at BS2 and then shows a potential positive peak (up to -25.3 ‰) in the basal part of S2 (~ 40 – 50 m). Another rapid increase of $\delta^{13}\text{C}_{\text{org}}$ (up to -25.1 ‰) is observed in the basal part of S3 (~ 100 – 110 m). Accordingly, the carbon isotopic fractionations between carbonate and organic matter ($\Delta^{13}\text{C}_{\text{carb-org}}$) are in the basal part range between 25.5 ‰ and 28.6 ‰.

The $\delta^{34}\text{S}_{\text{CAS}}$ shows a decrease (from 37.8 ‰ to 26.3 ‰) followed by an increase (from 26.3 ‰ to 37.5 ‰) in S1. The $\delta^{34}\text{S}_{\text{CAS}}$ shows an abrupt decline (down to 13.7 ‰) at BS2 and then fluctuates between 11.0 ‰ and 26.3 ‰ in the lower part of S2 (~ 40 – 70 m). The $\delta^{34}\text{S}_{\text{CAS}}$ increases (from 12.0 ‰ to 27.7 ‰) in the upper part of S2 (~ 70 – 100 m) and then scatters between 24.8 ‰ and 31.0 ‰ in S3. The $\delta^{34}\text{S}_{\text{CRS}}$ first decreases (from

12.2 ‰ to -10.1 ‰), then increases to and remains around ~ 0 ‰ in S1. The $\delta^{34}\text{S}_{\text{CRS}}$ shows an abrupt decline (down to ~ -12 ‰) at BS2 and remains constant in the lower part of S2 (~ 40 – 70 m). The $\delta^{34}\text{S}_{\text{CRS}}$ increases (from ~ -12 ‰ to 5.4 ‰) in the upper part of S2 (~ 70 – 100 m) and then ranges between -13.8 ‰ and -0.8 ‰ in S3. The sulphur isotopic fractionations between CAS and CRS ($\Delta^{34}\text{S}_{\text{CAS-CRS}}$) range between 10.3 ‰ and 44.5 ‰.

The major and trace element contents are listed in Table 2 and plotted in Figure 3. The Sc, Zr, Th, Al, Ti and SiO₂ contents show a maximum peak value in the lower part of S2 (~ 40 – 60 m) and exhibit a decreasing trend in the upper part of S2 (~ 60 – 100 m). Another high peak value can be observed in the lower part of S3 (~ 100 – 120 m).

REE + Y anomalies are calculated using the following formulae: $\text{Ce}/\text{Ce}^* = \text{Ce}_N/[\text{Pr}_N \times (\text{Pr}_N/\text{Nd}_N)]$, $\text{Eu}/\text{Eu}^* = \text{Eu}_N/(\text{Sm}_N^2 \times \text{Tb}_N)^{1/3}$, and $\text{La}/\text{La}^* = \text{La}_N/[\text{Pr}_N \times (\text{Pr}_N/\text{Nd}_N)^2]$ (Lawrence & Kamber, 2006). The concentrations of the elements with the subscript 'N' have been normalized to Post-Archaean Australian Shale (PAAS) (Taylor & McLennan, 1985). The REE + Y contents are listed in Table 3 and plotted in Figure 4. The total REE contents range between 10.9 ppm and 74.1 ppm, with slightly negative Ce anomalies ($\text{Ce}/\text{Ce}^* = 0.85 \pm 0.07$), no Y anomalies ($\text{Y}_N/\text{Ho}_N = 1.00 \pm 0.05$), no Eu anomalies ($\text{Eu}/\text{Eu}^* = 0.95 \pm 0.07$), no/slight light-REE (LREE) depletion ($\text{Pr}_N/\text{Sm}_N = 0.89 \pm 0.09$), and moderate high-REE (HREE) depletion ($\text{Sm}_N/\text{Yb}_N = 1.55 \pm 0.31$, $\text{Pr}_N/\text{Yb}_N = 1.37 \pm 0.28$).

5. Discussion

5.a. Fidelity of geochemical records for contemporaneous seawater

During diagenesis, Sr is often expelled from sedimentary carbonates; in contrast, Mn is preferentially incorporated; thus, carbonates with $\text{Mn}/\text{Sr} < 10$ are indicative of minimum diagenetic alteration (Derry *et al.* 1992; Kaufman & Knoll, 1995). All the Mn/Sr ratios of the Tangwangzhai carbonates are very low (< 2) (Table 2), suggesting limited post-depositional alteration. The lack of obvious covariations between Mn/Sr and $\delta^{13}\text{C}_{\text{carb}}/\delta^{13}\text{C}_{\text{org}}/\delta^{34}\text{S}_{\text{CAS}}$ further supports that the carbon and sulphur isotopic compositions were not altered significantly by diagenesis (Fig. 5a, b, c). Oxygen isotopic composition is also sensitive to diagenesis, which can reduce the $\delta^{18}\text{O}$ values in sediments because of isotopic exchange with meteoric or hydrothermal fluids; thus, $\delta^{18}\text{O}$ values below -10 ‰ are considered signs of strong alteration (Kaufman & Knoll, 1995). All the $\delta^{18}\text{O}$ values from the Tangwangzhai carbonates are above -10 ‰, and there is no covariation between $\delta^{18}\text{O}$ and $\delta^{13}\text{C}_{\text{carb}}$, also implying no diagenetic control of $\delta^{13}\text{C}_{\text{carb}}$ (Table 1; Fig. 5d).

Previous studies indicated that meteoric diagenesis can be negligible for bulk carbonate $\delta^{34}\text{S}_{\text{CAS}}$ owing to the much higher sulphate contents in the sediments compared with the diagenetic fluid (Gill *et al.* 2008), and the $\delta^{34}\text{S}_{\text{CAS}}$ did not change with progressive burial diagenesis (Fichtner *et al.* 2017). Bacterial sulphate reduction during early diagenesis may affect the $\delta^{34}\text{S}_{\text{CAS}}$ (Kampschulte & Strauss, 2004), but CAS studies of modern carbonate sediments indicate minimal alteration of bulk $\delta^{34}\text{S}_{\text{CAS}}$, which is unlikely to result in increases in $\delta^{34}\text{S}_{\text{CAS}}$ greater than 4 ‰ (Lyons *et al.* 2004; Rennie & Turchyn, 2014). Recent studies have indicated that secondary sulphate derived from sulphide oxidation in the pore water, outcrop and laboratory would be incorporated into the CAS, and secondary atmospheric sulphate (SAS) could also be added to exposed carbonates in desert

Table 1. The carbon and sulphur isotopic compositions in carbonate from the Tangwanzhai section

Sample	Depth (m)	$\delta^{13}\text{C}_{\text{carb}}$ (‰)	$\delta^{18}\text{O}_{\text{carb}}$ (‰)	$\delta^{13}\text{C}_{\text{org}}$ (‰)	$\delta^{34}\text{S}_{\text{CAS}}$ (‰)	$\delta^{34}\text{S}_{\text{CRS}}$ (‰)	CAS-S (ppm)	CRS-S (ppm)	$\Delta^{34}\text{S}_{\text{CAS-CRS}}$ (‰)	$\Delta^{13}\text{C}_{\text{carb-org}}$ (‰)
09TWZ-1	0.00	0.22	-7.63	-28.90	31.8	4.2	32.90	1.01	27.6	29.12
09TWZ-2	1.00	0.16	-8.18							
09TWZ-4	2.90	-0.22	-7.78	-26.40	36.4	12.2	279.69	223.66	24.2	26.18
09TWZ-5	3.80	-0.23	-7.76							
09TWZ-8	6.20	-0.24	-7.94							
09TWZ-13	9.00	-0.30	-7.64	-26.70	37.8	3.0	74.04	0.11	34.8	26.40
09TWZ-20	12.00	-0.27	-7.37							
09TWZ-28	16.20	-0.50	-8.01	-26.40	34.3	-10.1	74.04	33.98	44.5	25.90
09TWZ-33	18.10	0.06	-7.62							
09TWZ-40	21.40	0.15	-7.97	-27.60	28.8	1.2	106.94	1.95	27.6	27.75
09TWZ-46	24.00	-0.24	-8.04							
09TWZ-52	27.00	0.31	-7.69	-27.50	26.3	-0.8	57.58	8.19	27.1	27.81
09TWZ-59	30.40	0.30	-7.70	-27.00	35.0	-0.2	24.68	1.93	35.2	27.30
09TWZ-63	33.40	0.40	-7.42							
09TWZ-65	37.10	0.27	-7.43	-26.70	37.5	0.3	123.39	19.55	37.2	26.97
09TWZ-70	39.60	0.55	-7.42							
09TWZ-72	40.30	0.86	-7.69	-26.50	37.5	1.4	49.36	11.63	36.1	27.36
09TWZ-73	40.50	0.42	-8.16	-25.10						25.52
09TWZ-74	41.00	0.71	-7.48	-26.20	24.3	-14.2	90.49	25.18	38.5	26.91
09TWZ-76	42.30	0.66	-7.98							
09TWZ-78	43.90	1.30	-7.25	-26.60	26.7	-13.1	271.47	242.07	39.8	27.90
09TWZ-79	44.50	1.68	-7.51							
09TWZ-80	47.00	0.19	-7.73	-25.30	13.7	-12.7	74.04	5.01	26.4	25.49
09TWZ-82	48.20	0.69	-7.64							
09TWZ-83	50.20	1.18	-7.60	-26.50	29.0	-11.6	106.94	5.07	40.6	27.68
09TWZ-86	51.70	0.96	-7.47							
09TWZ-88	52.70	1.08	-7.51	-26.80	17.0	-11.1	123.39	11.58	28.1	27.88
09TWZ-90	53.70	0.96	-7.18							
09TWZ-92	54.70	0.57	-7.45	-26.10	15.1	-13.7	189.20	4.21	28.7	26.67
09TWZ-94	55.80	-0.13	-7.81							
09TWZ-96	56.80	0.65	-7.47	-26.20	22.6	-11.9	90.49	10.31	34.5	26.85
09TWZ-98	58.30	0.68	-7.54							
09TWZ-100	59.30	0.99	-7.43	-26.50	21.3	2.4	164.52	1.26	18.9	27.49

(Continued)

Table 1. (Continued)

Sample	Depth (m)	$\delta^{13}\text{C}_{\text{carb}}$ (‰)	$\delta^{18}\text{O}_{\text{carb}}$ (‰)	$\delta^{13}\text{C}_{\text{org}}$ (‰)	$\delta^{34}\text{S}_{\text{CAS}}$ (‰)	$\delta^{34}\text{S}_{\text{CRS}}$ (‰)	CAS-S (ppm)	CRS-S (ppm)	$\Delta^{34}\text{S}_{\text{CAS-CRS}}$ (‰)	$\Delta^{13}\text{C}_{\text{carb-org}}$ (‰)
09TWZ-101	60.00	0.74	-7.51							
09TWZ-103	61.50	0.52	-7.45	-27.00	28.2	-11.5	98.71	8.18	39.7	27.52
09TWZ-105	62.50	0.82	-7.25							
09TWZ-107	63.50	0.12	-7.39	-25.70	21.4	11.1	115.17	2.66	10.3	25.82
09TWZ-109	64.50	0.56	-7.61							
09TWZ-110	65.20	0.58	-7.14	-26.40	28.2	-12.7	65.81	1.91	41.0	26.98
09TWZ-112	66.20	0.24	-7.72							
09TWZ-114	68.20	0.13	-7.36	-26.80	17.6	-7.6	189.20	236.92	25.2	26.93
09TWZ-116	70.20	0.08	-7.37							
09TWZ-118	72.20	0.19	-7.81	-26.20	12.0	-3.7	131.62	5.96	15.7	26.39
09TWZ-120	74.20	0.41	-7.32							
09TWZ-123	77.20	0.53	-7.58	-27.40	19.6	-1.3	156.30	3.68	21.0	27.93
09TWZ-126	80.20	0.02	-7.32							
09TWZ-129	82.20	0.29	-7.58	-27.00	24.5	5.4	74.04	91.99	19.1	27.29
09TWZ-130	83.20	0.32	-8.00							
09TWZ-132	85.40	0.89	-7.70	-26.50						27.39
09TWZ-133	86.40	0.68	-7.45							
09TWZ-134	87.90	0.53	-7.72	-26.60						27.13
09TWZ-136	89.90	0.67	-8.45							
09TWZ-138	91.90	0.75	-7.82	-27.80	30.4	-8.9	65.81	1.70	39.3	28.55
09TWZ-140	93.90	0.80	-7.75							
09TWZ-142	94.90	0.65	-7.94							
09TWZ-145	96.40	0.41	-8.05							
09TWZ-149	98.40	0.30	-7.86	-28.20	27.7	-2.6	90.49	7.26	30.3	28.50
09TWZ-150	98.90	-3.48	-8.05							
09TWZ-152	99.90	-0.95	-7.84	-27.30	24.8	-13.8	82.26	28.21	38.6	26.35
09TWZ-155	101.40	-0.10	-8.15							
09TWZ-158	102.50	0.29	-8.18	-26.70						26.99
09TWZ-159	102.70	0.27	-7.89							
09TWZ-162	104.10	0.65	-7.88	-25.00	27.3	-7.5	197.43	75.35	34.7	25.65
09TWZ-165	106.30	0.36	-7.97	-27.10	26.6	-8.2	189.20	127.04	34.8	27.46
09TWZ-169	108.30	0.90	-7.76							
09TWZ-173	110.50	0.70	-7.79	-27.40	28.5	-1.1	222.11	15.26	29.6	28.10

(Continued)

Table 1. (Continued)

Sample	Depth (m)	$\delta^{13}\text{C}_{\text{carb}}$ (‰)	$\delta^{18}\text{O}_{\text{carb}}$ (‰)	$\delta^{13}\text{C}_{\text{org}}$ (‰)	$\delta^{34}\text{S}_{\text{CAS}}$ (‰)	$\delta^{34}\text{S}_{\text{CRS}}$ (‰)	CAS-S (ppm)	CRS-S (ppm)	$\Delta^{34}\text{S}_{\text{CAS-CRS}}$ (‰)	$\Delta^{13}\text{C}_{\text{carb-org}}$ (‰)
09TWZ-175	112.40	0.41	-8.05	-26.50	27.4	-0.8	205.66	54.46	28.2	26.91
09TWZ-176	114.40	1.13	-7.69							
09TWZ-177	116.40	1.19	-7.67	-26.80	31.0	-2.8	205.66	24.08	33.7	27.99
09TWZ-178	118.40	-0.16	-7.75							
09TWZ-179	120.40	0.81	-7.75	-26.30	25.1	-6.0	213.88	24.01	31.1	27.11

environments, both of which might affect the $\delta^{34}\text{S}_{\text{CAS}}$ (Marenco *et al.* 2008; Wotte *et al.* 2012a; Peng *et al.* 2014). In this study, the samples were effectively leached by NaClO and NaCl prior to the CAS extraction (see Section 3), excluding the non-CAS sulphate. No covariance between $\delta^{34}\text{S}_{\text{CAS}}$, CAS and CRS concentrations suggests no prominent two end members mixing between oxidized pyrite and primary sulphate (Fig. 5e, f, g), further supporting that insufficient pyrite is oxidized. In addition, most samples have very low CRS contents (mostly <10 ppm), which are much lower than CAS contents (mostly >70 ppm) (Fig. 2). The low CRS contents suggest that (1) the primary pyrite was limited, and little of it could be oxidized and affected the CAS; (2) almost all primary pyrite (>90%) was oxidized and affected the CAS, but such a high pyrite reoxidation ratio seems impossible either during the early diagenesis or during the CAS extraction. Samples 09TWZ-4 (36.4 ‰), 09TWZ-78 (26.7 ‰) and 09TWZ-114 (17.6 ‰) have high CRS contents (>200 ppm) (Fig. 2), and the corresponding CAS also shows relatively high contents, suggesting potential S addition to the CAS in these samples during diagenesis. Overall, in the lower part of the Chaomidian Formation (TST of S2: ~40–70 m), CRS concentrations of most samples are <5 ppm (Fig. 2), implying that the pyrite may have contributed minimal sulphate to the CAS. Therefore, the decline in $\delta^{34}\text{S}_{\text{CAS}}$ within the TST of S2 was not caused by the oxidation of pyrite, which thus reflects the isotopic composition change of ambient seawater.

Some elements (e.g. Al, Ti, Sc, Zr, Th) are conservative in normal depositional conditions, and also hardly react with aqueous phase and other minerals in normal depositional conditions, so they can be transferred and preserved almost quantitatively in the sediments, and generally used to trace detrital fraction (Taylor & McLennan, 1985; Webb & Kamber, 2000). REE + Y patterns in the carbonate can monitor their input sources (e.g. continental, riverine, hydrothermal) and depositional conditions (Nothdurft *et al.* 2004; Frimmel, 2009), but the diagenesis in anoxic pore water may lead to depletion of both LREE and HREE (Haley *et al.* 2004). In the Tangwangzhai carbonates, no HREE nor LREE depletion is observed (Fig. 4). Furthermore, the low Mn/Sr ratios (<2) and the lack of covariation of Mn/Sr-Pr_N/Yb_N also indicate limited diagenetic alteration of REE in the Tangwangzhai carbonates (Table 2; Fig. 5h).

In summary, the carbon and sulphur isotope compositions and trace elements are pristine, representing those of the contemporary seawater at the depositional locality.

5.b. Oceanic geochemistry in North China during the late Cambrian

Trace elements were analysed by acetic acid (1 M) dissolution, and the low concentrations of Sc (mostly <2 ppm), Zr (<3 ppm) and

Th (mostly <1 ppm) suggest that the impact from the detritus was eliminated effectively (Table 2). The Tangwangzhai carbonate shows relatively flat REE + Y patterns with no obvious Ce, Eu, Y or LREE anomalies (Fig. 4), similar to the REE + Y patterns observed in estuaries / coastal seas where the REE + Y characteristics are strongly impacted by riverine input (Elderfield *et al.* 1990; Lawrence & Kamber, 2006; Censi *et al.* 2007; Frimmel, 2009). The moderate HREE depletion is always related to the contribution from suspended load in the river (Nothdurft *et al.* 2004; Prego *et al.* 2012; Bayon *et al.* 2015; de Campos & Enzweiler, 2016). Previous sedimentological studies suggested the late Cambrian carbonate and shale in North China were deposited in subtidal environments (e.g. shallow subtidal, deep subtidal, shoreface/shoal) (Chen *et al.* 2011, 2012), which is consistent with the estuarine/coastal conditions indicated by REE + Y. In this case, the multiple sea-level fluctuations might play an important role in the chemostratigraphic records because they could change the proportioning between terrigenous/riverine input and primary seawater, and even cause interruptions in deposition.

Al, Ti, SiO₂, Sc, Zr and Th contents can be used to track continental detritus in the sediments (Hild & Brumsack, 1998; Tribouillard *et al.* 2006). Maximum peaks of Al, Ti and SiO₂ contents appear in the lower part of S2 (~40–60 m) and lower part of S3 (~100–120 m) (Fig. 3), suggesting a rapid increase in terrigenous influence; there is a decreasing trend in the upper part of S2 (~60–100 m) (Fig. 3), suggesting a decrease in terrigenous influence. Sc, Zr and Th were leached by acetic acid, which represents only a very small part of continental detritus, but their stratigraphic variations mostly appear like those of Al, Ti and SiO₂. This observation is consistent with the petrology features and sedimentary sequences: the seawater and sediments were greatly influenced by terrigenous input in the TST, where the sediments contain more shale interlayers; the terrigenous influence was weakened during the HST, where the sediments contain fewer shale interlayers (Chen *et al.* 2011).

The variations of $\delta^{13}\text{C}_{\text{carb}}$ and $\delta^{34}\text{S}_{\text{CAS}}$ show correspondences to the sea-level changes. In the Gushan Formation, the $\delta^{13}\text{C}_{\text{carb}}$ values in the lower part (TST of S1: ~0–20 m) are lower than those in the upper part (HST of S1: ~20–40 m) (Fig. 2); in the lower part of the Chaomidian Formation (TST of S2: ~40–70 m), the $\delta^{13}\text{C}_{\text{carb}}$ values show a gradual decrease following a rapid increase at the bottom, and then the $\delta^{13}\text{C}_{\text{carb}}$ increases to ~+0.5 ‰ in the middle part of the Chaomidian Formation (HST of S2: ~70–100 m). The $\delta^{13}\text{C}_{\text{carb}}$ variations represent the changes of DIC isotope in the ocean, which were controlled by the input (predominantly terrestrial weathering input) and output (predominantly carbonate and organic carbon burial) fluxes and their respective isotopes in the popular carbon

Table 2. The major and trace element contents in carbonate from the Tangwanzhai section

Sample	Depth (m)	SiO ₂ (%)	TiO ₂ (%)	Al ₂ O ₃ (%)	MnO (%)	Sc (ppm)	Sr (ppm)	Zr (ppm)	Th (ppm)	Mn/Sr
09TWZ-1	0.00	0.97	0.02	0.38	0.03	0.63	528.79	2.66	0.33	0.44
09TWZ-8	6.20					9.78	342.14	2.60	0.91	
09TWZ-20	12.00					1.70	318.28	2.62	0.33	
09TWZ-40	21.40	3.09	0.04	0.87	0.03	1.38	455.12	2.63	0.60	0.51
09TWZ-63	33.40					1.36	436.54	2.33	0.53	
09TWZ-70	39.60					1.58	337.58	2.62	0.98	
09TWZ-80	47.00	5.66	0.08	1.48	0.04	1.21	218.50	2.31	0.61	1.42
09TWZ-86	51.70					6.27	305.71	2.26	1.08	
09TWZ-88	52.70	4.21	0.07	1.01	0.05	1.27	306.24	2.63	0.95	1.26
09TWZ-92	54.70	5.22	0.09	1.38	0.05	1.87	270.05	2.66	0.94	1.43
09TWZ-96	56.80	9.53	0.15	2.68	0.03	2.81	212.19	2.27	1.42	1.10
09TWZ-100	59.30	5.30	0.08	1.36	0.03	1.60	314.36	2.27	1.02	0.74
09TWZ-105	62.50					1.44	366.88	2.32	1.21	
09TWZ-109	64.50					1.95	333.08	2.30	1.81	
09TWZ-114	68.20	4.95	0.08	1.31	0.04	1.23	307.26	2.29	0.83	1.01
09TWZ-118	72.20	5.01	0.09	1.39	0.03	1.48	279.49	2.29	1.05	0.83
09TWZ-123	77.20	5.01	0.08	1.38	0.03	1.07	307.41	2.28	0.84	0.76
09TWZ-126	80.20	3.50	0.05	1.06	0.02	0.85	438.82	2.28	0.67	0.35
09TWZ-130	83.20					1.95	352.32	2.31	0.62	
09TWZ-134	87.90	4.98	0.07	1.23	0.03	1.45	371.96	2.28	0.58	0.62
09TWZ-138	91.90	3.95	0.05	0.89	0.02	0.98	259.99	2.27	0.63	0.60
09TWZ-142	94.90					0.84	414.08	2.63	0.63	
09TWZ-149	98.40	0.51	0.02	0.21	0.03	0.80	277.22	2.43	0.59	0.84
09TWZ-152	99.90	1.50	0.04	0.40	0.06	2.51	240.03	2.38	1.54	1.94
09TWZ-155	101.40					0.61	283.82	2.76	0.61	
09TWZ-158	102.50	1.81	0.01	0.12	0.04	0.31	239.20	2.62	0.60	1.30
09TWZ-159	102.70	2.19	0.02	0.30	0.04	0.13	235.07	2.52	0.26	1.32
09TWZ-165	106.30	3.62	0.02	0.25	0.04	0.37	297.06	2.54	0.29	1.04
09TWZ-173	110.50	7.60	0.12	1.48	0.04	2.12	281.43	2.57	0.82	1.10
09TWZ-175	112.40	3.83	0.05	0.74	0.07	0.84	312.91	2.56	0.40	1.73
09TWZ-179	120.40	6.02	0.11	1.43	0.04	2.49	278.07	2.60	0.67	1.11

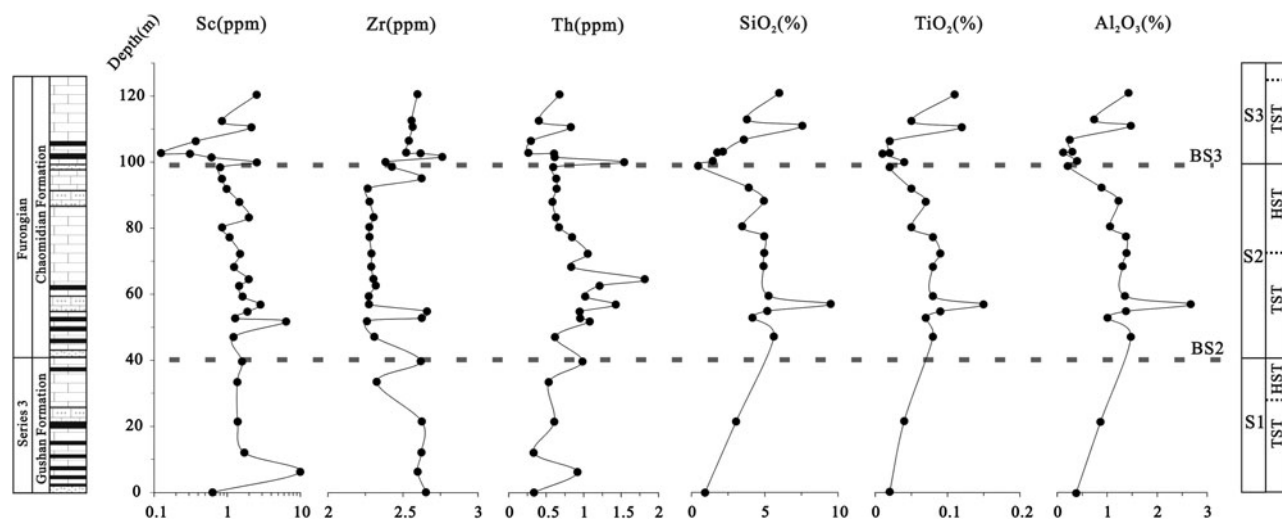


Fig. 3. Major and trace element content variations from late Cambrian carbonate in the Tangwangzhai section.

cycling models (Hayes *et al.* 1999; Kump & Arthur, 1999). The change of terrestrial input flux or isotope could impact the DIC isotope directly, but the effect might be diluted in a large DIC pool (or amplified in a small pool). Generally, terrestrial sources influence the coastal DIC by input of weathering carbon that contained weathered inorganic carbon and remineralized organic carbon, and the average weathering carbon input is ^{13}C -depleted (~ -5 ‰) (Hayes *et al.* 1999; Kump & Arthur, 1999). Despite the lack of evidence of wide land biomass during the Cambrian, weathering of exposed high organic shale could provide considerable ^{13}C -depleted remineralized organic carbon to the river and ocean. Therefore, the enhanced terrigenous input would result in the lower/decreasing $\delta^{13}\text{C}_{\text{carb}}$ in TST, while higher/increasing $\delta^{13}\text{C}_{\text{carb}}$ in the HST suggests weakening of the terrigenous influence under this environment.

The $\delta^{34}\text{S}_{\text{CAS}}$ shows a decreasing trend in the lower part of the Gushan Formation (TST of S1: ~ 0 –20 m), and also shows a decrease and fluctuations in a relatively low range of values (~ 11.0 –26.3 ‰) in the lower part of the Chaomidian Formation (TST of S2: ~ 40 –60 m), both of which are attributed to the enhanced terrigenous influence. The $\delta^{34}\text{S}_{\text{CAS}}$ variations represent the changes of sulphate isotope in the ocean, which are mainly controlled by the input (predominantly terrestrial weathering input) flux and output (predominantly evaporate and pyrite burial) flux and their respective isotopes (Canfield, 2004). The change of terrestrial input flux and/or its isotopes influences the ocean sulphate isotope directly. Like carbon, this effect is more pronounced for a small sulphate pool than a large sulphate pool of seawater. The isotopic composition of the riverine input sulphate is primarily set by the relative proportions of dissolved sulphate evaporate and oxidized pyrite, and the average weathering input sulphate was regarded as relatively isotopically light in sulphur (~ 6 –10 ‰) (Walker, 1986; Arthur, 2000). Recent models for the late Cambrian sulphur cycling generally assumed ~ 6 ‰ as the riverine input sulphur isotopic compositions (Hurtgen *et al.* 2009; Gill *et al.* 2011). We acknowledge that the local sulphate weathering input is also largely impacted by the local sediments, which was likely to cause more ^{34}S -enriched weathering input. For instance, Fike & Grotzinger (2008) suggested ^{34}S -enriched weathering input (~ 30 ‰) during the Ediacaran–Cambrian transition by using the ‘rapid recycling’ hypothesis, which predicted that young

sedimentary rocks were subject to rapid weathering relative to older strata because the younger rocks were more exposed to erosion at the earth surface (Berner, 2006). For the late Cambrian weathering, however, the younger middle Cambrian strata were likely to be the weathering source, in which the $\delta^{34}\text{S}$ values of pyrite in sediments from several regions are all lower than 20 ‰ in the middle Cambrian (Gill *et al.* 2011; Loyd *et al.* 2012; Wotte *et al.* 2012b; Guo *et al.* 2014). Hence, we exclude a strongly ^{34}S -enriched weathering input (>20 ‰) in case of ‘rapid recycling’ during the late Cambrian. Therefore, the enhanced terrigenous input would reduce the $\delta^{34}\text{S}$ of coastal seawater to <20 ‰ in TST, especially in the context of the low SO_4^{2-} concentration in the late Cambrian (Hurtgen *et al.* 2009; Gill *et al.* 2011); the $\delta^{34}\text{S}_{\text{CAS}}$ shows a gradual increase back to the HST in both S1 and S2, implying the weakening of terrigenous influences.

The invasion of ^{13}C -depleted/ ^{34}S -depleted deep seawater probably provides an alternative explanation during the TST. For a coastal condition that was shallow and nearshore, however, the influence from deep water would be considerably weaker than terrigenous influence. In addition, the influence from deep water remains largely unexplored. The carbon isotopic gradients show variations in different basins: the seawater was more ^{13}C -enriched in the deep ocean in the Missouri intrashelf basin (Schiffbauer *et al.* 2017), while it was more ^{13}C -depleted in the deep ocean in the Huanan basin (Li *et al.* 2018). Gill *et al.* (2011) suggested a widespread euxinia in the deep ocean, where the H_2S might be more ^{34}S -depleted compared with sulphate in the shallow water. However, the synchronous pyrite records in deep water suggested that the $\delta^{34}\text{S}$ of H_2S was >20 ‰ for a long time, which did not necessarily cause the $\delta^{34}\text{S}_{\text{CAS}}$ to reduce to <20 ‰ as we observed in the Tangwangzhai section. Besides, the widespread euxinia for the SPICE event remains controversial (Wotte & Strauss, 2015).

Pasquier *et al.* (2017) also suggested a potential relationship between sea-level and sulphur isotopic records in the sediments: sedimentation rates might increase in low sea-level, which would reduce connectivity between sedimentary pore waters and overlying seawaters, and cause enhanced $\delta^{34}\text{S}_{\text{SO}_4}$ and $\delta^{34}\text{S}_{\text{py}}$ in closed pore water through ongoing microbial sulphate reduction. This hypothesis contradicts our observation. Therefore, in our case, the terrigenous influence linked to the sea-level change would be a reasonable explanation: the lower/decreasing $\delta^{13}\text{C}_{\text{carb}}$ and

Table 3. The REE+Y contents (ppm) in carbonate from the Tangwanzhai section

Sample	Depth (m)	La	Ce	Pr	Nd	Sm	Eu	Gd	Tb	Dy	Y	Ho	Er	Tm	Yb	Lu	REE	Ce/Ce*	Eu/Eu*	Y _N /Ho _N	Pr _N /Sm _N	Sm _N /Yb _N	Pr _N /Yb _N
09TWZ-1	0.00	2.09	4.21	0.51	1.99	0.46	0.08	0.43	0.07	0.43	2.74	0.09	0.25	0.04	0.23	0.04	10.91	0.92	0.84	1.12	0.69	1.03	0.72
09TWZ-8	6.20	10.89	25.71	4.06	18.47	4.21	0.90	3.60	0.55	2.81	13.94	0.51	1.21	0.16	0.93	0.14	74.14	0.83	1.13	1.00	0.61	2.29	1.39
09TWZ-20	12.00	6.28	12.84	1.91	8.16	1.76	0.34	1.55	0.23	1.23	6.42	0.23	0.57	0.08	0.46	0.07	35.68	0.83	1.01	1.02	0.68	1.96	1.34
09TWZ-40	21.40	2.87	5.76	0.73	2.82	0.57	0.09	0.49	0.08	0.41	2.19	0.08	0.21	0.03	0.17	0.03	14.33	0.88	0.81	1.01	0.80	1.68	1.36
09TWZ-63	33.40	3.28	6.53	0.97	3.91	0.72	0.14	0.68	0.10	0.50	2.75	0.10	0.24	0.03	0.20	0.03	17.42	0.78	0.99	1.05	0.85	1.83	1.56
09TWZ-70	39.60	8.70	18.39	2.24	8.49	1.61	0.31	1.53	0.24	1.31	7.37	0.26	0.68	0.09	0.56	0.09	44.48	0.90	0.97	1.04	0.87	1.46	1.27
09TWZ-80	47.00	4.32	8.48	1.32	5.28	0.88	0.15	0.79	0.11	0.58	3.11	0.11	0.27	0.04	0.21	0.03	22.56	0.75	0.93	1.05	0.94	2.15	2.01
09TWZ-86	51.70	12.11	25.26	3.41	12.84	2.39	0.46	2.17	0.33	1.84	10.17	0.36	0.92	0.13	0.78	0.11	63.09	0.81	0.99	1.04	0.90	1.55	1.39
09TWZ-88	52.70	7.27	14.48	1.80	6.82	1.25	0.23	1.17	0.18	0.96	5.42	0.18	0.49	0.07	0.42	0.06	35.35	0.89	0.93	1.10	0.91	1.51	1.37
09TWZ-92	54.70	6.74	14.02	1.93	7.43	1.37	0.22	1.21	0.18	0.97	5.15	0.19	0.48	0.07	0.40	0.06	35.26	0.81	0.83	1.02	0.89	1.72	1.53
09TWZ-96	56.80	5.52	11.42	1.61	6.45	1.16	0.21	1.03	0.16	0.84	4.08	0.16	0.41	0.06	0.36	0.05	29.42	0.83	0.94	0.92	0.87	1.65	1.44
09TWZ-100	59.30	5.98	12.53	1.71	6.54	1.20	0.21	1.07	0.15	0.83	4.44	0.16	0.42	0.06	0.36	0.06	31.29	0.81	0.94	1.01	0.89	1.70	1.52
09TWZ-105	62.50	6.64	13.35	1.78	6.97	1.29	0.24	1.13	0.18	0.98	4.91	0.19	0.47	0.07	0.41	0.06	33.76	0.85	0.96	0.96	0.87	1.59	1.38
09TWZ-109	64.50	7.83	17.30	2.19	8.23	1.60	0.29	1.45	0.22	1.29	6.71	0.26	0.66	0.10	0.59	0.09	42.09	0.86	0.94	0.97	0.86	1.38	1.18
09TWZ-114	68.20	4.52	9.30	1.23	4.53	0.83	0.15	0.79	0.12	0.67	3.74	0.13	0.35	0.05	0.31	0.05	23.01	0.81	0.91	1.04	0.93	1.39	1.28
09TWZ-118	72.20	6.61	13.12	1.82	6.85	1.17	0.22	1.12	0.17	0.93	4.80	0.18	0.46	0.07	0.41	0.06	33.18	0.79	0.95	0.98	0.98	1.45	1.42
09TWZ-123	77.20	3.92	7.12	0.91	3.43	0.61	0.11	0.57	0.08	0.46	2.43	0.09	0.23	0.03	0.20	0.03	17.79	0.85	0.91	0.99	0.94	1.53	1.44
09TWZ-126	80.20	2.42	4.40	0.57	2.06	0.38	0.07	0.35	0.06	0.32	1.71	0.06	0.17	0.02	0.14	0.02	11.04	0.79	0.91	1.00	0.95	1.36	1.30
09TWZ-130	83.20	4.17	8.05	1.14	4.18	0.75	0.15	0.67	0.10	0.53	2.70	0.10	0.26	0.04	0.22	0.03	20.39	0.75	1.05	0.95	0.96	1.73	1.66
09TWZ-134	87.90	4.80	8.47	1.05	3.83	0.65	0.11	0.61	0.09	0.51	2.60	0.10	0.27	0.04	0.23	0.04	20.80	0.86	0.89	0.93	1.01	1.44	1.45
09TWZ-138	91.90	4.11	7.07	0.89	3.20	0.57	0.11	0.55	0.08	0.43	2.28	0.09	0.22	0.03	0.18	0.03	17.55	0.83	0.98	0.98	0.98	1.60	1.56
09TWZ-142	94.90	3.60	6.08	0.76	2.80	0.55	0.09	0.45	0.07	0.36	1.99	0.07	0.18	0.03	0.15	0.02	15.19	0.86	0.86	1.06	0.87	1.83	1.59
09TWZ-149	98.40	5.44	10.04	1.10	4.12	0.75	0.14	0.79	0.12	0.71	3.90	0.14	0.38	0.05	0.30	0.05	24.11	0.99	0.91	1.01	0.93	1.25	1.16
09TWZ-152	99.90	11.39	24.46	2.60	9.34	1.81	0.39	1.88	0.31	1.88	10.78	0.39	1.10	0.16	1.08	0.16	56.94	0.98	1.04	1.00	0.90	0.85	0.77

(Continued)

Table 3. (Continued)

Sample	Depth (m)	La	Ce	Pr	Nd	Sm	Eu	Gd	Tb	Dy	Y	Ho	Er	Tm	Yb	Lu	REE	Ce/Ce*	Eu/Eu*	Y _N /Ho _N	Pr _N /Sm _N	Sm _N /Yb _N	Pr _N /Yb _N
09TWZ-155	101.40	5.26	9.62	1.10	4.19	0.81	0.15	0.79	0.12	0.71	3.90	0.14	0.37	0.05	0.32	0.05	23.68	0.96	0.93	0.99	0.85	1.31	1.11
09TWZ-158	102.50	3.97	7.67	0.87	3.37	0.64	0.12	0.61	0.10	0.56	2.93	0.12	0.29	0.04	0.27	0.04	18.68	0.98	0.95	0.91	0.86	1.19	1.02
09TWZ-159	102.70	3.16	6.29	0.69	2.45	0.50	0.09	0.47	0.07	0.43	2.25	0.09	0.23	0.03	0.20	0.03	14.72	0.94	0.95	0.94	0.87	1.26	1.09
09TWZ-165	106.30	10.18	17.22	2.12	7.58	1.28	0.24	1.20	0.18	0.93	4.67	0.18	0.41	0.06	0.35	0.05	41.96	0.84	0.98	0.97	1.04	1.87	1.95
09TWZ-173	110.50	9.49	16.40	2.25	8.48	1.52	0.30	1.40	0.21	1.15	5.37	0.22	0.51	0.07	0.46	0.06	42.51	0.80	1.02	0.90	0.93	1.70	1.58
09TWZ-175	112.40	6.91	11.74	1.49	5.35	0.99	0.20	0.91	0.13	0.70	3.64	0.14	0.35	0.05	0.30	0.04	29.31	0.82	1.03	0.96	0.94	1.67	1.57
09TWZ-179	120.40	7.68	12.98	1.59	5.69	1.12	0.22	1.03	0.17	0.96	4.81	0.19	0.49	0.07	0.46	0.07	32.72	0.84	1.00	0.93	0.89	1.23	1.10

REE + Y anomalies are calculated by the following formulae: Ce/Ce* = Ce_N/Pr_N × (Pr_N/Nd_N); Eu/Eu* = Eu_N/Sm_N² × Tb_N^{1/3}; La/La* = La_N/Pr_N × (Pr_N/Nd_N)². The concentrations of elements with the subscript N have been normalized to Post-Archaean Australian Shale (PAAS).

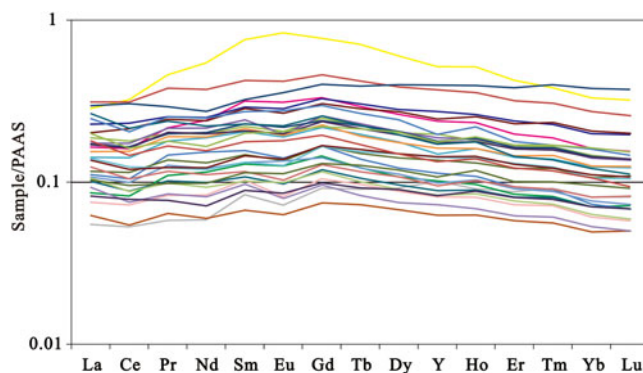


Fig. 4. (Colour online) REE + Y patterns from late Cambrian carbonate in the Tangwanzhai section.

δ³⁴S_{CAS} in the TST was attributed to enhanced terrigenous influence; and the higher/increasing δ¹³C_{carb} and δ³⁴S_{CAS} in the HST was due to weakened terrigenous influence.

5.c. The SPICE records in North China

The base of the Furongian Series is defined by the first appearance datum (FAD) of the cosmopolitan agnostoid *Glyptagnostus reticulatus* in Hunan, China (Peng *et al.* 2004). Previous work discovered the coexistence of *Chuangia* and *G. reticulatus* in South China (Peng, 1987), providing for the first time a crucial trilobitic correlation between North China and South China. Therefore, the base of the *Chuangia* Zone was proposed to correlate to the FAD of *G. reticulatus*, which is the base of the Furongian Series in North China (e.g. Zhang & Jell, 1987; Zhu & Wittke, 1989; Zhang, 2003; Ng *et al.* 2014a). A new Cambrian correlation scheme suggested a thin *Prochuangia-Paracoosia* trilobite zone between the *Chuangia* Zone and *Neodrepanura* Zone, and the base of the Furongian Series should be in the middle of the *Prochuangia-Paracoosia* zone (Peng, 2009a, b). This implies that the base of the Furongian Series should be stratigraphically slightly lower than the base of the *Chuangia* Zone. However, the *Prochuangia-Paracoosia* zone is missing in some areas of North China. In any case, the base of the Furongian Series in North China should be near the base of the *Chuangia* Zone. Accordingly, the carbon isotope positive excursion in some locations in North China was proposed as the SPICE record, which ends near the bottom of the *Changshania* Zone (Zhu *et al.* 2004; Chen *et al.* 2011; Bagnoli *et al.* 2014; Ng *et al.* 2014a, b). Compared with other areas, the SPICE in North China is all recorded in a relatively thin carbonate succession (~5–20 m), and shows reduced δ¹³C_{carb} excursions (<2.5 ‰), with peak values lower than the average range of 4–5% (Ng *et al.* 2014a, b).

In addition, conodont *Furnihina quadrata* and *Furnishina longibasis* first occur close to the FAD of *G. reticulatus* in the Paibi stratotype section, which would also be a proxy to distinguish the base of the Furongian Series (Qi *et al.* 2006). In the Tangwanzhai section, *F. quadrata* and *F. longibasis* first occur near the base of the *Chuangia* Zone, which can confirm the base of the Furongian Series (Bagnoli *et al.* 2014). Therefore, the mild positive δ¹³C_{carb} excursion (~15 m thick) starting near the base of the *Chuangia* Zone has been identified as the SPICE records in the Tangwanzhai section (Zhu *et al.* 2004; Bagnoli *et al.* 2014), which is also observed in this study (Fig. 2). A negative excursion (low to 0.19 ‰) is observed in the middle part of the SPICE curve, which

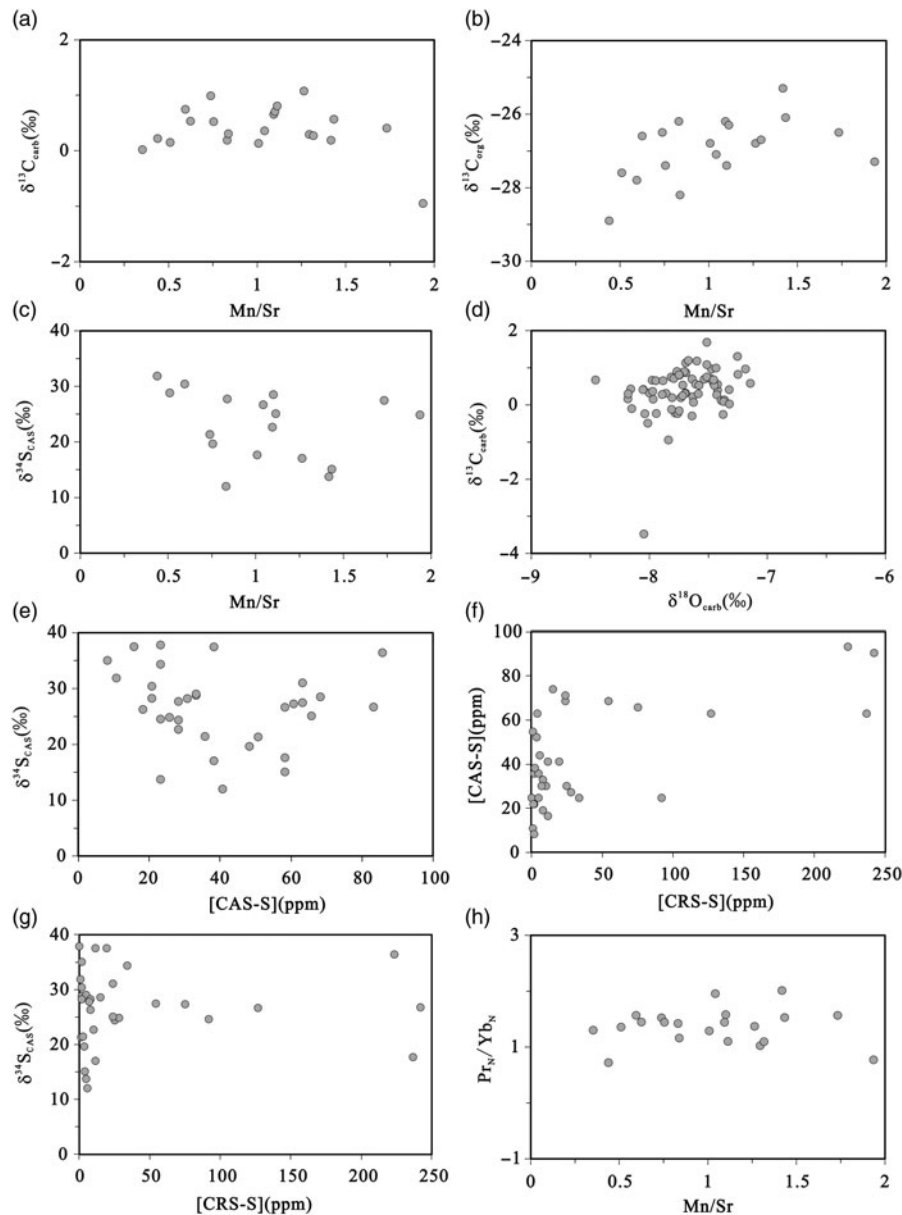


Fig. 5. Isotopic and elemental cross-plots for late Cambrian carbonate in the Tangwangzhai section. (a) $\delta^{13}\text{C}_{\text{carb}}$ -Mn/Sr; (b) $\delta^{13}\text{C}_{\text{org}}$ -Mn/Sr; (c) $\delta^{34}\text{S}_{\text{CAS}}$ -Mn/Sr; (d) $\delta^{13}\text{C}_{\text{carb}}$ - $\delta^{18}\text{O}_{\text{carb}}$; (e) $\delta^{34}\text{S}_{\text{CAS}}$ -[CAS-S]; (f) [CAS-S]-[CRS-S]; (g) $\delta^{34}\text{S}_{\text{CAS}}$ -[CRS-S]; (h) Pr_N/Yb_N -Mn/Sr.

was also reported in the same section (Bagnoli *et al.* 2014), the Shuanqiao section in North China (Ng *et al.* 2014b) and the Wa'ergang and Paibi sections in South China (Saltzman *et al.* 2000; Peng *et al.* 2004). A similar positive excursion of $\delta^{13}\text{C}_{\text{org}}$ that corresponds to the SPICE has also been reported in many sections throughout the world (Gill *et al.* 2011; Saltzman *et al.* 2011). A potential positive peak of $\delta^{13}\text{C}_{\text{org}}$ is present corresponding to the $\delta^{13}\text{C}_{\text{carb}}$ peak (Fig. 2), which likely provides additional chemostratigraphic correlation evidence for the SPICE in North China. However, we acknowledge that more $\delta^{13}\text{C}_{\text{org}}$ data are needed in order to validate the excursion.

A positive sulphur isotope (including $\delta^{34}\text{S}_{\text{CAS}}$ and $\delta^{34}\text{S}_{\text{py}}$) excursion in phase with the SPICE, which is considered as a useful chemostratigraphic correlation tool, was found in several geographically diverse sections (Gill *et al.* 2007, 2011). Generally, the $\delta^{34}\text{S}_{\text{CAS}}/\delta^{34}\text{S}_{\text{py}}$ excursions co-vary with the SPICE $\delta^{13}\text{C}_{\text{carb}}$ excursions. The $\delta^{34}\text{S}_{\text{CAS}}$ continuously increases to >40 ‰ and then

decreases, in which the peak is close to (or slightly pre-dates) the $\delta^{13}\text{C}_{\text{carb}}$ peak (Gill *et al.* 2007, 2011). However, a few SPICE records show no continuous $\delta^{34}\text{S}_{\text{CAS}}$ increase prior to the $\delta^{13}\text{C}_{\text{carb}}$ peak, and some even show $\delta^{34}\text{S}_{\text{CAS}}$ decline with the onset of the $\delta^{13}\text{C}_{\text{carb}}$ increase (Fig. 6) (Hurtgen *et al.* 2009; Gill *et al.* 2011; Wotte & Strauss, 2015). In these records, a peak point of $\delta^{34}\text{S}_{\text{CAS}}$ (~ 48 ‰) was reported in Kazakhstan, which is considered to be correlated to the $\delta^{34}\text{S}_{\text{CAS}}$ positive excursion (Wotte & Strauss, 2015), but the other records show no conventional $\delta^{34}\text{S}_{\text{CAS}}$ peak from Newfoundland and Queensland (Fig. 6) (Hurtgen *et al.* 2009; Gill *et al.* 2011). In this study, we observe no $\delta^{34}\text{S}_{\text{CAS}}/\delta^{34}\text{S}_{\text{py}}$ increase prior to the $\delta^{13}\text{C}_{\text{carb}}$ peak either: the $\delta^{34}\text{S}_{\text{CAS}}/\delta^{34}\text{S}_{\text{py}}$ show relatively high values (~ 40 ‰) around the onset of the $\delta^{13}\text{C}_{\text{carb}}$ increase, but then abruptly decline at BS2 and fluctuate in a relatively low value range (~ 10 – 20 ‰) (Figs 2, 6).

The erosion surface at BS2 may cause the SPICE records to be partially missing at the bottom of the SPICE (Chen *et al.* 2011, 2012).

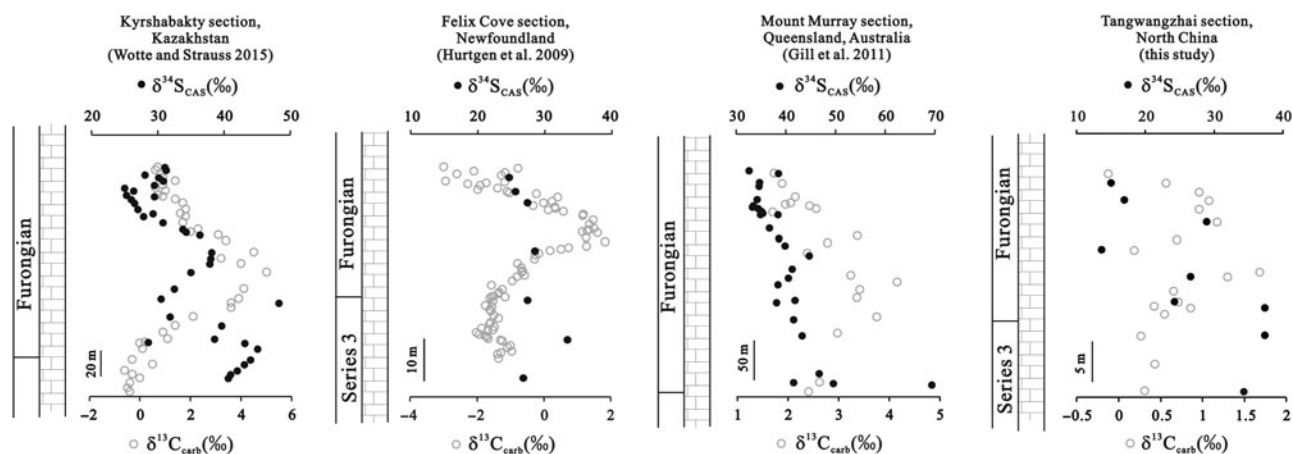


Fig. 6. Comparison of SPICE records with abnormal $\delta^{34}\text{S}_{\text{CAS}}$ variations. (a) A peak point of $\delta^{34}\text{S}_{\text{CAS}}$ (~48‰) was reported prior to the $\delta^{13}\text{C}_{\text{carb}}$ peak in Kazakhstan, but the $\delta^{34}\text{S}_{\text{CAS}}$ positive excursion is not obvious (Wotte & Strauss, 2015); (b, c) no conventional $\delta^{34}\text{S}_{\text{CAS}}$ peak in the records from Newfoundland and Queensland (Hurtgen *et al.* 2009; Gill *et al.* 2011); (d) no $\delta^{34}\text{S}_{\text{CAS}}/\delta^{34}\text{S}_{\text{py}}$ increase prior to $\delta^{13}\text{C}_{\text{carb}}$ peak in North China (this study).

More importantly, the coastal seawater was greatly influenced by the ^{34}S -depleted terrigenous input after the submergence of subaerial unconformity (i.e. TST in S2), which would dilute or even obscure the $\delta^{34}\text{S}$ positive excursion of the open seawater. Therefore, the $\delta^{34}\text{S}_{\text{CAS}}$ abruptly declines at the BS2, and could not resume the positive excursion pattern throughout the SPICE event, reflecting long-term and strong terrigenous influences. The $\delta^{13}\text{C}_{\text{carb}}$ would also be influenced by ^{13}C -depleted terrigenous input, but the reservoir of DIC in the Furongian seawater was much larger than that of sulphate, so the mixing $\delta^{13}\text{C}$ would modestly decrease, and the $\delta^{13}\text{C}_{\text{carb}}$ excursion only show the magnitude reduction rather than depletion in North China.


These abnormal $\delta^{34}\text{S}_{\text{CAS}}$ patterns may reflect different degrees of local influence, assuming positive $\delta^{34}\text{S}$ excursions represent the primary change of the open seawater during SPICE. Up to now, there is insufficient evidence to say that the other records with declining $\delta^{34}\text{S}_{\text{CAS}}$ at the onset of SPICE excursion were also related to the terrigenous input like that in North China. We acknowledge that the controlling factors on these $\delta^{34}\text{S}$ records need to be thoroughly evaluated within their geological contexts. At the very least, the variable $\delta^{34}\text{S}_{\text{CAS}}$ records reflect a more sensitive sulphur reservoir, supporting the low sulphate concentrations in the late Cambrian ocean.

6. Conclusions

We report new data of carbon and sulphur isotopes and trace elements in the late Cambrian stratum in North China, which represent the heterogeneity in carbon and sulphur isotopic compositions in the Furongian seawater. The REE and trace elements results support coastal conditions with multiple sedimentary sequences. The REE + Y patterns are relatively flat with no obvious Ce, Eu, Y or LREE anomalies, but they show moderate HREE depletion, suggesting shallow estuarial/coastal conditions that likely were significantly affected by riverine input. Variations of Al, Ti, SiO_2 , Sc, Zr and Th contents were used to track detritus from continents, which confirm that the seawater and sediments were greatly influenced in the TST, and the influence would weaken in the HST. The terrigenous input would also affect the carbon and sulphur isotopic compositions of the ocean. Both the $\delta^{13}\text{C}_{\text{carb}}$ and the $\delta^{34}\text{S}_{\text{CAS}}$ decrease and fluctuate within a range of relatively low values in the TST because of the large

influence from ^{13}C -depleted and ^{34}S -depleted terrigenous input; they then recover when the terrigenous influences weaken in the HST.

A positive $\delta^{13}\text{C}_{\text{carb}}$ excursion and a potential positive $\delta^{13}\text{C}_{\text{org}}$ peak are observed near the base of the *Chuangia* Zone; this $\delta^{13}\text{C}_{\text{carb}}$ excursion would be the SPICE record, as suggested by previous studies. This SPICE record in North China may be influenced by the subaerial unconformity and strongly terrigenous input: the former would cause the carbon and sulphur isotope records to be partially missing; the latter with depleted $\delta^{13}\text{C}$ and $\delta^{34}\text{S}$ would cause the amplitude of the positive $\delta^{13}\text{C}_{\text{carb}}$ excursion to be reduced, and the positive $\delta^{34}\text{S}_{\text{CAS}}$ excursion even to be obscured in North China. The variable $\delta^{34}\text{S}_{\text{CAS}}$ records further reflect a sensitive sulphur reservoir, supporting the low sulphate concentrations in the late Cambrian ocean which is vulnerable to local influences.

Author ORCIDs.  Jing Huang 0000-0003-0158-4151

Acknowledgments. This research is supported by the Natural Science Foundation of China (41673002, 41890842, 41520104007, 41721002, 41330102), the Key Research Program of Frontier Sciences, CAS (QYZDY-SSW-DQC031) and the 111 Project, and the Fundamental Research Funds for the Central Universities. We thank Prof. Luo Kunli, Li Chao and Zhang Qirui for their help with the field and lab work.

References

- Ahlberg PER, Axheimer N, Babcock LE, Eriksson ME, Schmitz B and Terfelt F (2009) Cambrian high-resolution biostratigraphy and carbon isotope chemostratigraphy in Scania, Sweden: first record of the SPICE and DICE excursions in Scandinavia. *Lethaia* **42**, 2–16.
- Álvoro JJ, Ferretti A, González-Gómez C, Serpagli E, Tortello MF, Vecoli M and Vizcaíno D (2007) A review of the Late Cambrian (Furongian) palaeogeography in the western Mediterranean region, NW Gondwana. *Earth-Science Reviews* **85**, 47–81.
- Arnold GL, Brunner B, Müller IA and Roy H (2014) Modern applications for a total sulfur reduction distillation method – what's old is new again. *Geochemical Transactions* **15**, 4. doi: 10.1186/1467-4866-15-4.
- Arthur MA (2000) Volcanic contributions of the carbon and sulfur geochemical cycles and global change. In *Encyclopedia of Volcanoes* (eds H Sigurdsson, B Houghton, S McNutt, H Rymer and J Stix), pp. 1045–56. Amsterdam: Academic Press.

- Bagnoli G, Qi YP, Zuo JX, Du SX, Liu SC and Zhang ZQ** (2014) Integrated biostratigraphy and carbon isotopes from the Cambrian Tangwangzhai section, North China. *Palaeoworld* **23**, 112–24.
- Bayon G, Toucanne S, Skonieczny C, André L, Bermell S, Cheron S, Dennielou B, Etoubleau J, Freslon N, Gauchery T and Germain Y** (2015) Rare earth elements and neodymium isotopes in world river sediments revisited. *Geochimica et Cosmochimica Acta* **170**, 17–38.
- Berner RA** (2006) GEOCARBSULF: a combined model for Phanerozoic atmospheric O₂ and CO₂. *Geochimica et Cosmochimica Acta* **70**, 5653–64.
- Canfield DE** (2004) The evolution of the Earth surface sulfur reservoir. *American Journal of Science* **304**, 839–61.
- Censi P, Sprovieri M, Saiano F, Di Geronimo SI, Larocca D and Placenti F** (2007) The behaviour of REEs in Thailand's Mae Klong estuary: suggestions from the Y/Ho ratios and lanthanide tetrad effects. *Estuarine, Coastal and Shelf Science* **71**, 569–79.
- Chen J, Chough SK, Han Z, and Lee J-H** (2011) An extensive erosion surface of a strongly deformed limestone bed in the Gushan and Chaomidian formations (late Middle Cambrian to Furongian), Shandong Province, China: sequence-stratigraphic implications. *Sedimentary Geology* **233**, 129–49.
- Chen J, Chough SK, Lee J-H and Han Z** (2012) Sequence-stratigraphic comparison of the upper Cambrian Series 3 to Furongian succession between the Shandong region, China and the Taebaek area, Korea: high variability of bounding surfaces in an epeiric platform. *Geosciences Journal* **16**, 357–79.
- Chough SK, Lee HS, Woo J, Chen J, Choi DK, Lee SB, Kang I, Park TY and Han Z** (2010) Cambrian stratigraphy of the North China Platform: revisiting principal sections in Shandong Province, China. *Geosciences Journal* **14**, 235–68.
- Cowan CA, Fox DL, Runkel AC and Saltzman MR** (2005) Terrestrial-marine carbon cycle coupling in ~500-m.y.-old phosphatic brachiopods. *Geology* **33**, 661–4.
- Dahl TW, Boyle RA, Canfield DE, Connelly JN, Gill BC, Lenton TM and Bizzarro M** (2014) Uranium isotopes distinguish two geochemically distinct stages during the later Cambrian SPICE event. *Earth and Planetary Science Letters* **401**, 313–26.
- de Campos FF and Enzweiler J** (2016) Anthropogenic gadolinium anomalies and rare earth elements in the water of Atibaia River and Anhumas Creek, Southeast Brazil. *Environmental Monitoring and Assessment* **188**, 1–18.
- Derry LA, Kaufman AJ and Jacobsen SB** (1992) Sedimentary cycling and environmental change in the Late Proterozoic: evidence from stable and radiogenic isotopes. *Geochimica et Cosmochimica Acta* **56**, 1317–29.
- Elderfield H, Upstill-Goddard R and Sholkovitz ER** (1990) The rare earth elements in rivers, estuaries, and coastal seas and their significance to the composition of ocean waters. *Geochimica et Cosmochimica Acta* **54**, 971–91.
- Elrick M, Rieboldt S, Saltzman M and McKay RM** (2011) Oxygen-isotope trends and seawater temperature changes across the Late Cambrian Steptoean positive carbon-isotope excursion (SPICE event). *Geology* **39**, 987–90.
- Fichtner V, Strauss H, Immenhauser H, Buhl D, Neuser RD and Niedermayr A** (2017) Diagenesis of carbonate associated sulfate. *Chemical Geology* **258**, 338–53.
- Fike DA and Grotzinger JP** (2008) Paired sulfate–pyrite $\delta^{34}\text{S}$ approach to understanding the evolution of the Ediacaran–Cambrian sulfur cycle. *Geochimica et Cosmochimica Acta* **72**, 2636–48.
- Frimmel HE** (2009) Trace element distribution in Neoproterozoic carbonates as palaeoenvironmental indicator. *Chemical Geology* **463**, 61–75.
- Garrels RM and Lerman A** (1981) Phanerozoic cycles of sedimentary carbon and sulfur. *Proceedings of the National Academy of Sciences* **78**, 4652–6.
- Gill BC, Lyons TW and Frank TD** (2008) Behavior of carbonate-associated sulfate during meteoric diagenesis and implications for the sulfur isotope paleoproxy. *Geochimica et Cosmochimica Acta* **72**, 4699–711.
- Gill BC, Lyons TW and Saltzman MR** (2007) Parallel, high-resolution carbon and sulfur isotope records of the evolving Paleozoic marine sulfur reservoir. *Palaeogeography, Palaeoclimatology, Palaeoecology* **256**, 156–73.
- Gill BC, Lyons TW, Young SA, Kump LR, Knoll AH and Saltzman MR** (2011) Geochemical evidence for widespread euxinia in the Later Cambrian ocean. *Nature* **469**, 80–3.
- Glumac B** (2011) High-resolution stratigraphy and correlation of Cambrian strata using carbon isotopes: an example from the southern Appalachians, USA. *Carbonates Evaporites* **26**, 287–97.
- Glumac B and Mutti LE** (2007) Late Cambrian (Steptoean) sedimentation and responses to sea-level change along the northeastern Laurentian margin: insights from carbon isotope stratigraphy. *Geological Society of America Bulletin* **119**, 623–36.
- Glumac B and Spivak-Birndorf ML** (2002) Stable isotopes of carbon as an invaluable stratigraphic tool: an example from the Cambrian of the northern Appalachians USA. *Geology* **30**, 563–6.
- Guo Q, Straus H, Zhao Y, Yang X, Peng J, Yang Y and Deng Y** (2014) Reconstructing marine redox conditions for the transition between Cambrian Series 2 and Cambrian Series 3, Kaili area, Yangtze Platform: evidence from biogenic sulfur and degree of pyritization. *Palaeogeography, Palaeoclimatology, Palaeoecology* **398**, 114–53.
- Haley BA, Klinkhammer GP and McManus J** (2004) Rare earth elements in pore waters of marine sediments. *Geochimica et Cosmochimica Acta* **68**, 1265–79.
- Hayes JM, Straus H and Kaufman AJ** (1999) The abundance of ^{13}C in marine organic matter and isotopic fractionation in the global biogeochemical cycle of carbon during the past 800 Ma. *Chemical Geology* **161**, 103–25.
- Hild E and Brumsack HJ** (1998) Major and minor element geochemistry of Lower Aptian sediments from the NW German Basin (core Hoheneggelsen KB 40). *Cretaceous Research* **19**, 615–33.
- Hough ML, Shields GA, Evins LZ, Strauss H, Henderson RA and Mackenzie I** (2006) A major sulphur isotope event at c. 510 Ma: a possible anoxia-extinction-volcanism connection during the Early–Middle Cambrian transition? *Terra Nova* **18**, 257–63.
- Hurtgen MT, Pruss SB and Knoll AH** (2009) Evaluating the relationship between the carbon and sulfur cycles in the later Cambrian ocean: an example from the Port au Port Group, western Newfoundland, Canada. *Earth and Planetary Science Letters* **281**, 288–97.
- Kampschulte A and Strauss H** (2004) The sulfur isotopic evolution of Phanerozoic seawater based on the analysis of structurally substituted sulfate in carbonates. *Chemical Geology* **204**, 255–86.
- Kaufman AJ and Knoll AH** (1995) Neoproterozoic variations in the C-isotopic composition of seawater — stratigraphic and biogeochemical implications. *Precambrian Research* **73**, 27–49.
- Kump LR and Arthur MA** (1999) Interpreting carbon-isotope excursions: carbonates and organic matter. *Chemical Geology* **161**, 181–98.
- Lawrence M and Kamber B** (2006) The behaviour of the rare earth elements during estuarine mixing – revisited. *Marine Chemistry* **100**, 147–61.
- Lee J-H, Chen J, Choh S-J, Lee D-J, Han Z and Chough SK** (2014) Furongian (Late Cambrian) sponge–microbial maze-like reefs in the North China Platform. *Palaaios* **29**, 27–37.
- Lee J-H, Chen J and Chough SK** (2010) Palaeoenvironmental implications of an extensive macerate microbialite bed in the Furongian Chaomidian Formation, Shandong Province, China. *Palaeogeography, Palaeoclimatology, Palaeoecology* **297**, 621–32.
- Lee J-H, Chen J and Chough SK** (2012) Demise of an extensive biostromal microbialite in the Furongian (late Cambrian) Chaomidian Formation, Shandong Province, China. *Geosciences Journal* **16**, 275–84.
- Li D, Zhang X, Hu D, Chen X, Huang W, Zhang X, Li M, Qin L, Peng S and Shen Y** (2018) Evidence of a large $\delta^{13}\text{C}_{\text{carb}}$ and $\delta^{13}\text{C}_{\text{org}}$ depth gradient for deep-water anoxia during the late Cambrian SPICE event. *Geology* **46**, 631–4.
- Lloyd SJ, Marengo PJ, Hagadorn JW, Lyons TW, Kaufman AJ, Sour-Tovar F and Corsetti FA** (2012) Sustained low marine sulfate concentrations from the Neoproterozoic to the Cambrian: insights from carbonates of northwestern Mexico and eastern California. *Earth and Planetary Science Letters* **339–340**, 79–94.
- Lyons TW, Walter LM, Gellatly AM, Martini AM and Blake RE** (2004) Sites of anomalous organic remineralization in the carbonate sediments of South Florida, USA: the sulfur cycle and carbonate-associated sulfate. In *Sulfur Biogeochemistry: Past and Present* (eds JP Amend, KJ Edwards & KJ Lyons), pp. 161–76. Geological Society of America, Special Paper no. 379.
- Maloof AC, Porter SM, Moore JL, Dudás FÖ, Bowring SA, Higgins JA, Fike DA and Eddy MP** (2010) The earliest Cambrian record of animals and ocean geochemical change. *Geological Society of America Bulletin* **122**, 1731–74.

- Marengo PJ, Corsetti FA, Hammond DE, Kaufman AJ and Bottjer DJ (2008) Oxidation of pyrite during extraction of carbonate associated sulfate. *Chemical Geology* **247**, 124–132.
- Ng T-W, Botting JP, Yuan J-L and Lin J-P (2015) New discoveries of Cambrian pelmatozoan echinoderm ossicles from North China. *Palaeoworld* **24**, 438–44.
- Ng T-W, Yuan J-L and Lin J-P (2014a) The North China Steptoean positive carbon isotope event: new insights towards understanding a global phenomenon. *Geobios* **47**, 371–87.
- Ng T-W, Yuan J-L and Lin J-P (2014b) The North China Steptoean positive carbon isotope excursion and its global correlation with the base of the Paibian Stage (early Furongian Series), Cambrian. *Lethaia* **47**, 153–64.
- Nothdurft LD, Webb GE and Kamber BS (2004) Rare earth element geochemistry of Late Devonian reefal carbonates, Canning Basin, Western Australia: confirmation of a seawater REE proxy in ancient limestones. *Geochimica et Cosmochimica Acta* **68**, 263–83.
- Pasquier V, Sansjofre P, Rabineau M, Revillon S, Houghton J and Fike DA (2017) Pyrite sulfur isotopes reveal glacial-interglacial environmental changes. *Proceedings of the National Academy of Sciences* **114**, 5941–5.
- Peng S (1987) Early Late Cambrian stratigraphy and trilobite fauna of Taoyuan and Cili, Hunan. In *Collection of Postgraduate Theses of the Nanjing Institute of Geology and Palaeontology, Academic Sinica, No.1*. Jiangsu Science and Technology Publishing House, Nanjing, 53–134 (in Chinese with English summary).
- Peng S (2007) Historical review of trilobite research in China. In *Fabulous Fossils – 300 Years of Worldwide Research on Trilobites* (eds DG Mikulic, E Landing and J Kluessendorf), pp. 171–92. Albany, New York: New York State Museum Bulletin.
- Peng S (2009a) Review on the studies of Cambrian trilobite faunas from Jiangnan slope belt, south China, with notes on Cambrian correlation between south and north China. *Acta Palaeontologica Sinica* **48**, 437–42.
- Peng S (2009b) The newly-developed Cambrian biostratigraphic succession and chronostratigraphic scheme for South China. *Chinese Science Bulletin* **54**, 4161–70.
- Peng S, Babcock LE, Robison RA, Lin H, Rees MN and Saltzman MR (2004) Global standard stratotype-section and point (GSSP) of the Furongian Series and Paibian Stage (Cambrian). *Lethaia* **37**, 365–79.
- Peng S, Babcock LE, Zuo J, Zhu X, Lin H, Yang X, Qi Y, Bagnoli G and Wang L (2012) Global Standard Stratotype-Section and Point (GSSP) for the Base of the Jiangshanian Stage (Cambrian: Furongian) at Duibian, Jiangshan, Zhejiang, Southeast China. *Episodes* **35**, 462–77.
- Peng Y, Bao H, Pratt LM, Kaufman AJ, Jiang G, Boyd D, Wang Q, Zhou C, Yuan X, Xiao S and Loyd S (2014) Widespread contamination of carbonate-associated sulfate by present-day secondary atmospheric sulfate: evidence from triple oxygen isotopes. *Geology* **42**, 815–18.
- Prego R, Caetano M, Bernárdez P, Brito P, Ospina-Alvarez N and Vale C (2012) Rare earth elements in coastal sediments of the northern Galician shelf: influence of geological features. *Continental Shelf Research* **35**, 75–85.
- Qi YP, Bagnoli G and Wang ZH (2006) Cambrian conodonts across the pre-Furongian to Furongian interval in the GSSP section at Paibi, Hunan, South China. *Rivista Italiana di Paleontologia e Stratigrafia* **112**, 177–90.
- Rennie VCF and Turchyn AV (2014) The preservation of $\delta^{34}\text{S}_{\text{SO}_4}$ and $\delta^{18}\text{O}_{\text{SO}_4}$ in carbonate-associated sulfate during marine diagenesis: a 25 Myr test case using marine sediments. *Earth and Planetary Science Letters* **395**, 13–23.
- Saltzman MR, Cowan CA, Runkel AC, Runnegar B, Stewart MC and Palmer AR (2004) The Late Cambrian Spice ($\delta^{13}\text{C}$) event and the Sauk II-Sauk III regression: new evidence from Laurentian Basins in Utah, Iowa, and Newfoundland. *Journal of Sedimentary Research* **74**, 366–77.
- Saltzman MR, Ripperdan RL, Brasier MD, Lohmann KC, Robison RA, Chang WT, Peng S, Ergaliev EK and Runnegar B (2000) A global carbon isotope excursion (SPICE) during the Late Cambrian: relation to trilobite extinctions, organic-matter burial and sea level. *Palaeogeography, Palaeoclimatology, Palaeoecology* **162**, 211–23.
- Saltzman MR, Runnegar B and Lohmann KC (1998) Carbon isotope stratigraphy of Upper Cambrian (Steptoean Stage) sequences of the eastern Great Basin: record of a global oceanographic event. *Geological Society of America Bulletin* **110**, 285–97.
- Saltzman MR, Young SA, Kump LR, Gill BC, Lyons TW and Runnegar B (2011) Pulse of atmospheric oxygen during the late Cambrian. *Proceedings of the National Academy of Sciences* **108**, 3876–81.
- Schiffbauer JD, Huntley JW, Fike DA, Jeffrey MJ, Gregg JM and Shelton KL (2017) Decoupling biogeochemical records, extinction, and environmental change during the Cambrian SPICE event. *Science Advances* **3**, e1602158.
- Sial AN, Peralta S, Toselli AJ, Ferreira VP, Frei R, Parada MA, Pimentel MM and Pereira NS (2013) High-resolution stable isotope stratigraphy of the upper Cambrian and Ordovician in the Argentine Precordillera: carbon isotope excursions and correlations. *Gondwana Research* **24**, 330–48.
- Taylor SR and McLennan SM (1985) *The continental crust: its composition and evolution*. Oxford: Blackwell Scientific Publications.
- Tribouillard N, Algeo TJ, Lyons T and Riboulleau A (2006) Trace metals as paleoredox and paleoproductivity proxies: an update. *Chemical Geology* **232**, 12–32.
- Veizer J, Holser WT and Wilgus CK (1980) Correlation of $^{13}\text{C}/^{12}\text{C}$ and $^{34}\text{S}/^{32}\text{S}$ secular variations. *Geochimica et Cosmochimica Acta* **44**, 579–87.
- Walker JCG (1986) Global geochemical cycles of carbon, sulfur and oxygen. *Marine Geology* **70**, 159–74.
- Webb GE and Kamber BS (2000) Rare earth elements in Holocene reefal microbialites: a new shallow seawater proxy. *Geochimica et Cosmochimica Acta* **64**, 1557–64.
- Woods MA, Wilby PR, Leng MJ, Rushton AWA and Williams M (2011) The Furongian (late Cambrian) Steptoean Positive Carbon Isotope Excursion (SPICE) in Avalonia. *Journal of the Geological Society* **168**, 851–62.
- Wotte T, Shields-Zhou GA and Strauss H (2012a) Carbonate-associated sulfate: experimental comparisons of common extraction methods and recommendations toward a standard analytical protocol. *Chemical Geology* **326–327**, 132–44.
- Wotte T and Strauss H (2015) Questioning a widespread euxinia for the Furongian (Late Cambrian) SPICE event: indications from $\delta^{13}\text{C}$, $\delta^{18}\text{O}$, $\delta^{34}\text{S}$ and biostratigraphic constraints. *Geological Magazine* **152**, 1085–103.
- Wotte T, Strauss H, Fugmann A and Garbe-Schönberg D (2012b) Paired $\delta^{34}\text{S}$ data from carbonate-associated sulfate and chromium-reducible sulfur across the traditional Lower–Middle Cambrian boundary of W-Gondwana. *Geochimica et Cosmochimica Acta* **85**, 228–53.
- Zhang W-T (2003) Cambrian correlation between North America and China based on trilobite and conodont faunas. *Acta Palaeontologica Sinica* **42**, 305–16 (in Chinese and English bilingual).
- Zhang W-T and Jell PA (1987) *Cambrian trilobites of North China: Chinese Cambrian trilobites housed in the Smithsonian Institution*. Beijing: Science Press, pp. 1–322.
- Zhou Z-C, Willems H, Li Y and Luo H (2011) A well-preserved carbonate tempestite sequence from the Cambrian Gushan Formation, eastern North China Craton. *Palaeoworld* **20**, 1–7.
- Zhu M-Y, Zhang J-M, Li G-X and Yang A-H (2004) Evolution of C isotopes in the Cambrian of China: implications for Cambrian subdivision and trilobite mass extinctions. *Geobios* **37**, 287–301.
- Zhu Z-L and Wittke HW (1989) Upper Cambrian trilobites from Tangshan, Hebei Province, North China. *Palaeontologia Cathayana* **4**, 199–259.